

Organic Polymer Thin-Film Transistor Photosensors

Michael C. Hamilton, *Student Member, IEEE* and Jerzy Kanicki, *Senior Member, IEEE*

Abstract—We present our study of the effects of monochromatic illumination on the electrical performance of organic polymer thin-film transistors (OP-TFTs) and the use of these devices as photosensors. In the case of monochromatic illumination that is strongly absorbed by the polymer, the drain current of a device biased in the OFF-state is significantly increased and the threshold voltage is reduced. Light that is not strongly absorbed by the polymer has little effect on the electrical performance of the OP-TFTs. We explain these effects in terms of the photogeneration of excitons in the polymer channel region of the device. The density of excitons generated in the polymer depends on the energy of the incident photons, as well as on the irradiance level of the incident illumination. The photogenerated excitons subsequently dissociate into electrons and holes. The electrons can be trapped by positively charged states, thereby reducing the threshold voltage, while the photogenerated holes contribute to the excess photocurrent measured at the drain. To demonstrate the possible use of OP-TFTs as photosensors, we also present the responsivity, photosensitivity (signal-to-noise ratio), external quantum efficiency, noise-equivalent power, and specific detectivity of these devices. The dependence of these parameters on the incident photon energy and irradiance level is described.

Index Terms—Conjugated organic polymer, detectivity, noise-equivalent power, photodetector, photosensitivity, photosensor, phototransistor, quantum efficiency, responsivity, signal-to-noise ratio, thin-film transistor (TFT).

I. INTRODUCTION

ELECTRONIC and optoelectronic devices based on conjugated organic semiconductors, both small molecules and polymers, have been the subject of increased research over the past few years. The interest in devices such as organic light-emitting devices (OLEDs), organic thin-film transistors (OTFTs) and organic photodetectors arises from the promise of the tunability of the electrical and optical characteristics of the organic materials and processing advantages such as deposition at low temperature, over large areas, and by direct printing [1]–[4]. These advantages will allow organic electronic and optoelectronic devices to be used in applications and configurations that are difficult to achieve with inorganic materials (i.e., large area display and sensor arrays, fabrication on flexible substrates, or curved surfaces).

One interesting application of organic semiconducting materials is in photodetectors. These detectors can be classified

into two main groups: two-terminal photodiodes and three-terminal phototransistors. A number of groups have described conjugated organic polymer-based photodiodes in various configurations and excellent reviews can be found in [5]–[7]. Several groups have discussed organic photodiode structures utilizing a blend of different polymers [8], incorporating a composite of a small molecule (such as C₆₀) and a polymer [9]–[12], using a multilayer structure composed of alternating layers of various polymers [13], in a microcavity [14], and combined with hydrogenated amorphous silicon (a-Si:H) TFT addressing [15]. Still, other groups have reported two-terminal photodetectors in a lateral configuration based on a self-assembled layer of a DNA derivative [16] and which have been optimized for optical detection in the near infrared [17].

However, a much smaller number of groups have demonstrated the effects of illumination on the electrical performance of organic polymer thin-film transistors (OP-TFTs) or the use of these devices as photosensors, which is the subject of this paper. Zukawa *et al.* have demonstrated an organic heterojunction-based phototransistor [18]. Schön and Klock have shown the use of a pentacene-based metal-semiconductor field-effect transistor as a phototransistor [19]. While, Narayan *et al.* have described an organic polymer field-effect transistor that responds to light [20], [21].

It is important to understand the effects, as well as the underlying physics, of illumination on the electrical performance of these devices, since many of the proposed uses of OP-TFTs will involve the possible exposure of the device to light (i.e., as a sensor in a photodetector array or as driving circuitry in active matrix displays). Here, we present the results of our study of the electrical performance of OP-TFTs based on F8T2 [poly(9,9-dioctylfluorene-co-bithiophene)] alternating copolymer exposed to monochromatic illumination. We also report on the performance of these devices when used as photodetectors.

II. DEVICE STRUCTURE

The device used in the experiments described below is an inverted, defined-gate, gate-planarized, coplanar thin-film transistor that has been previously described [22]–[25]. The devices were fabricated on an oxidized silicon substrate to facilitate processing in standard microelectronic fabrication equipment. RF magnetron sputtered chromium (Cr) was used for the patterned gate electrode. Spin-coated and thermally-cured benzocyclobutene (BCB) was used as the gate-planarization layer and also functions as a gate insulator and plasma-enhanced chemical vapor deposition (PECVD) hydrogenated amorphous silicon nitride (a-SiN:H) was used as a second gate insulator layer resulting in a total gate insulator capacitance per unit area (C_{ins}^{\prime}) of 7.5×10^{-9} F/cm². Radio frequency (RF)

Manuscript received February 27, 2004; revised June 17, 2004. This work was supported by National Institute of Standards and Technology–Advanced Technology Project and the Department of Defense under a National Defense Science and Engineering Graduate Fellowship sponsored by the Air Force Office of Scientific Research and administered by the American Society for Engineering Education.

The authors are with the Department of Electrical Engineering and Computer Science, The University of Michigan, Ann Arbor, MI 48109 USA (e-mail: kanicki@eecs.umich.edu).

Digital Object Identifier 10.1109/JSTQE.2004.833972

magnetron sputtered indium tin oxide (ITO) was used as the source and drain electrodes. A 1-wt% solution of the organic semiconductor F8T2 dissolved in either xylenes or mesitylenes was spin-coated (in air) and cured in a vacuum oven at 90°C, providing a uniform film with an approximate thickness of 1000 Å. The channel lengths (L) of our devices range from 6 to 56 μm and channel widths (W) range from 56 to 116 μm . All samples are stored at room temperature, in air, with yellow ambient light.

III. EXPERIMENTAL SETUP

The transfer characteristics (drain current versus gate-to-source voltage, $I_D - V_{GS}$) and output characteristics (drain current versus drain-to-source voltage, $I_D - V_{DS}$) of the OP-TFT were measured in the dark and under various levels of monochromatic illumination at room temperature using a Karl Suss PM8 probe station and an HP4156 semiconductor parameter analyzer (using medium integration) controlled by Interactive Characterization Software (Metrics). A 200-W mercury xenon (HgXe) arc lamp (Oriel Instruments) was used as the illumination source. The incident wavelength and irradiance (or optical flux) from the HgXe lamp were controlled, using optical interference filters [full-width at half-maximum (FWHM) < 10 nm] and neutral density filters, to provide wavelengths from 435.8 to 690.7 nm and irradiance levels up to approximately 30 $\mu\text{W}/\text{cm}^2$ at the surface of the polymer film. After being optically filtered, the light passed through a fiber optic cable and a Mitutoyo microscope, which was used to focus the illumination to a spot size centered on the channel of the device, illuminating the entire channel. The irradiance was measured, at the same location where the device is placed in the light spot, using an International Light Si photodetector (SHD033) with a flat response filter and fiber optic probe connected to an International Light research radiometer (IL1700). All measurements were performed in ambient air at room temperature and we did not observe any dependence of the device performance on room humidity.

It is well known that the electrical characteristics of OP-TFTs exhibit shifts due to measurement (from the application of biases) and other stresses (such as illumination) [26], [27]. We have observed that the shifts in the electrical characteristics due to illumination are much more significant than the shifts due to repeated (i.e., back-to-back) measurement in the dark. To compensate for these shifts, while allowing the experiments to be carried out in a reasonable manner, we annealed the devices between measurement sets (15 min at 90 °C in a vacuum oven). The measurement sequence we have used is as follows. We anneal the device, as describe earlier. Then, we measure the dark transfer characteristics. The illumination is then switched on and within a few seconds, the illuminated transfer characteristics are measured. This is followed by another anneal, measurement in the dark, measurement under illumination and so on. Therefore, the calculated parameters (see Sections IV and V) were found by using the illuminated characteristics compared to the immediately preceding dark characteristics, with no annealing step between. The annealing procedure removed the shifts caused by measurement and illumination and allowed the device (and its

electrical characteristics) to return to the original state (i.e., similar OFF-state drain current, threshold voltage, and subthreshold slope) before proceeding with the next measurement set, thereby providing more reliable results. Though the perturbation of the devices can be fully removed at room temperature, the elevated temperature significantly speeds up the recovery.

Additionally, we should note that we measured the transfer characteristics from the ON-state to the OFF-state (i.e., from $V_{GS} = -40$ to 20 V). We chose this measurement method because it provides very reproducible data, with a variation in the ON-current of less than $\pm 5\%$ for the linear regime transfer characteristics for the same device measured back-to-back in the dark (without annealing between measurements). Therefore, this measurement procedure allows reliable comparison of the electrical performance of the device in the dark and under illumination.

The data presented in this paper was taken from two randomly chosen devices, one for the measurements using different wavelengths of incident illumination and one for different levels of irradiance. We have observed similar effects for all devices tested, and the device-to-device reproducibility is acceptable, given the current status of organic-based electronics. In several of the following plots, the data is noisy. We believe the noise is mainly due to the small signal amplitudes (or division by small signals for the case of the calculated parameters). The trends in the data presented here have been observed for all devices tested under these measurement conditions.

IV. DEVICE OPERATION

A. In The Dark

OP-TFTs based on F8T2 exhibit p-channel field-effect transistor behavior as can be seen from the threshold voltage-normalized transfer characteristics (drain current versus gate-to-source voltage—threshold voltage, I_D versus $V_{GS} - V_T$) shown in Fig. 1. We extract the linear regime field-effect mobility and threshold voltage from the linear regime transfer characteristics using the following equation, based on the MOSFET gradual channel approximation [28]:

$$I_D = -\mu_{FE} C_{\text{ins}} \frac{W}{L} \left[(V_{GS} - V_T) V_{DS} - \frac{V_{DS}^2}{2} \right] \quad (1)$$

or, for low V_{DS}

$$I_D = -\mu_{FE} C_{\text{ins}} \frac{W}{L} (V_{GS} - V_T) V_{DS}. \quad (2)$$

In these equations, μ_{FE} is the linear regime field-effect mobility (cm^2/Vs), C_{ins} is the gate insulator capacitance per unit area (F/cm^2), W is the channel width of the device, L is the channel length of the device, V_{GS} is the applied gate-to-source bias, V_{DS} is the applied drain-to-source bias, and V_T is the linear regime threshold voltage. We associate the negative value of the threshold voltage of the p-channel OP-TFTs with the density of positively charged states in the organic polymer, N_T , that must be overcome before the conductive channel, of accumulated holes, can form [29]. The subthreshold swing can be extracted from the linear regime transfer characteristics, in the

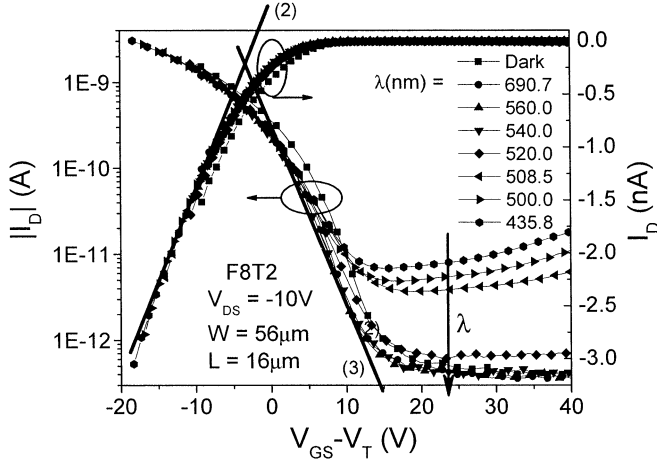


Fig. 1. Threshold voltage-normalized transfer characteristics of OP-TFT illuminated at different wavelengths/photon energies, with a constant optical flux of 5×10^{13} photons/cm²s. The straight lines are fits using (2) and (3).

transition region from the OFF-state to the ON-state, using the following equation:

$$I_D \propto 10^{-V_{GS}/S}. \quad (3)$$

In this equation, S is the subthreshold swing (V/decade). If we assume that the subthreshold swing can be associated with the density of deep bulk states in the organic semiconductor and interface states at the interface between the gate insulator and organic semiconductor, similar to the case for hydrogenated amorphous silicon (a-Si:H), then we can write [30]

$$S = \frac{kT}{q \log(e)} \left[1 + \frac{q d_{\text{ins}}}{\epsilon_{\text{ins}}} \left(\sqrt{\epsilon_{\text{semi}} N_{BS}} + q N_{SS} \right) \right] \quad (4)$$

where k , T , and q are the usual physical parameters; ϵ_{ins} and ϵ_{semi} are the dielectric constants of the insulator and semiconductor, respectively; d_{ins} is the effective thickness of the insulator; N_{BS} is the density of bulk states; and N_{SS} is the density of interface states. We note that an exact, analytical relation between the subthreshold swing in an organic field-effect device and the density of states in the organic material has yet to be developed. However, we believe that the subthreshold swing can be associated with the densities of bulk and interface states. For example, as the state densities increase, the device will turn on slower with applied gate bias and, therefore, have a larger subthreshold swing. This agrees with the general relation shown in (4).

From the linear regime transfer characteristics of a device in the dark, we find values of the linear regime field-effect mobility, threshold voltage, and subthreshold swing to be 5×10^{-4} cm²/Vs, -25 V, and 4.5 V/decade, respectively. For $S = 4.5$ V/decade, we find maximum values of surface state density N_{SS}^{max} and bulk state density N_{BS}^{max} to be 3.5×10^{12} cm²eV⁻¹ and 8.6×10^{18} cm³eV⁻¹, respectively. These values are comparable to values reported previously by us [22]–[25], [31] and others [32], [33].

B. Under Illumination

In the past, we have observed very strong effects of steady-state broadband illumination on the electrical performance of a-Si:H TFTs [34] and OP-TFTs based on F8T2 [25], [31]. In this paper, we examine the effects of illumination in more detail by exploring the response of the OP-TFTs to monochromatic illumination at different wavelengths and irradiance levels. In Fig. 1, we present the threshold-voltage normalized transfer characteristics (drain current versus gate-to-source voltage—threshold voltage, I_D versus $V_{GS} - V_T$). We plot the transfer characteristics in this manner in order to demonstrate that the major effects of the illumination are a reduction of the threshold voltage and an increase in the OFF-state drain current, while the field-effect mobility and subthreshold slope retain their same value as in the dark. More details on these effects, as well as the dependence on incident photon energy and irradiance are discussed in Sections V-A and B.

For the case of our devices, the most likely carrier generation process is through the exciton route. Photons with the proper energy are absorbed in the polymer, forming an exciton (i.e., a bound electron-hole pair). The exciton then diffuses to a dissociation site (i.e., defect, impurity, or surface state) and dissociates into a free electron and hole. Once generated, these free charge carriers move under the influence of the applied electric fields (from the applied V_{DS} and V_{GS}) and in opposite directions through the channel of the OP-TFT. Many of the electrons are trapped into, and neutralize positively charged traps (N_T) that contribute to the large negative threshold voltage, thereby reducing the threshold voltage. The photogenerated holes are collected at the drain electrode (by the corresponding transfer of an electron from the drain electrode into the valence band of the polymer). The drain current in the OFF-state is significantly increased, while a smaller increase in the drain current in the strong accumulation regime is observed. The significant increase of drain current in the OFF-state, when the device is under illumination, can be attributed to the enhancement of the carrier density in, and therefore the conductivity of, the channel of the device due to the photogeneration and dissociation of excitons in the polymer. When the device is operated in the strong accumulation regime, the relative effect of the illumination on the drain current is much smaller compared to the effect in the OFF-state. This can be explained by the overwhelming effect of the gate voltage on the concentration of accumulated carriers in the channel of the device, at the levels of illumination used in this study.

V. EXPERIMENTAL RESULTS

A. Dependence on Photon Energy

The response of the OP-TFTs to monochromatic illumination has been investigated by measuring the transfer characteristics of a device in the dark and under monochromatic illumination at various wavelengths. Fig. 1 shows the linear regime, threshold voltage-normalized, transfer characteristics of an OP-TFT in the dark and illuminated at seven wavelengths from 435.8 to 690.7 nm with a constant optical flux of approximately 5×10^{13} photons/cm²s incident on the surface of the polymer

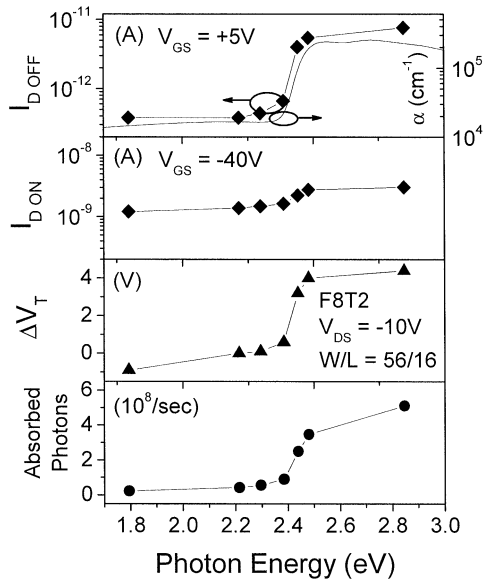


Fig. 2. Dependence of ON-state drain current, OFF-state drain current, and the change in threshold voltage on the energy of the incident photons. Extracted from the nonthreshold voltage-normalized transistor characteristics (not shown), using (2). Also shown is an estimation of the number of photons absorbed per second in the channel region of the device as a function of the photon energy.

film. In Fig. 2, we show the OFF-state drain current (extracted from Fig. 1) along with the absorption spectrum of the F8T2 polymer film. From Fig. 2, we can see that light with energy less than 2.4 eV (corresponding to the optical gap of the F8T2 films we used) is weakly absorbed and has little effect on the transfer characteristics, while light with higher energy (from 2.4 to 2.8 eV) is strongly absorbed, generating more excitons, and, therefore, has a much larger effect. Further evidence to support this explanation is found when we plot the number of absorbed photons versus the energy of the photons as in Fig. 2. The total number of absorbed photons was approximated using the incident photon flux, absorption coefficient (taken from Fig. 2), the effective area of the device ($W \times L$), and the thickness of the polymer.

The dependence of the change in threshold voltage [extracted from the linear regime transfer characteristics shown in Fig. 1 using (2)] on the energy of the incident photons is shown in Fig. 2. We can see that the change in threshold voltage is significantly larger for the strongly absorbed light, while little change is observed for light which is weakly absorbed. As explained earlier, some of the photogenerated electrons become trapped by and compensate positively charged traps N_T , reducing the threshold voltage, as we have observed for strongly absorbed light and as shown in Fig. 2 ($\Delta V_T = V_{T\text{illum}} - V_{T\text{dark}}$, therefore a positive ΔV_T corresponds to a reduction of the threshold voltage). N_T can be estimated from the threshold voltage to be approximately 10^{17} cm^{-3} . The change in threshold voltage of 4 V, corresponds to a change in N_T , ΔN_T , of approximately 10^{16} cm^{-3} . Further evidence that charge carrier trapping is taking place is provided by the fact that, after illumination, we are able to bring the devices back to their original state (i.e., the transfer characteristics shift back to the original state) by annealing the devices at elevated temperature. The trapped elec-

trons are detrapped faster at higher temperatures, causing the neutralized traps to become positively charged, thereby shifting the threshold voltage to its uncompensated value.

The subthreshold swing is not affected by the illumination, as can be seen in Fig. 1, where the subthreshold swings are equal for all of the characteristics in the dark and under illumination [note the slope of the line labeled (3)]. Since the subthreshold swing can be related to the density of states (both bulk states and interface states) as shown in (4), and since the subthreshold swing is not affected by the illumination, we conclude that the illumination does not affect the density of states of the polymer. Additionally, the field-effect mobility of the accumulated holes is not affected by the illumination, as can be seen from Fig. 1 [note the slope of the line labeled (2)]. This shows that the light has negligible effect on the electronic properties of the polymer film. Also, since the field-effect mobility is unchanged in these measurements, we conclude that the observed changes in the electrical characteristics are not a result of heating effects in the polymer.

It is important to note that the major effect of illumination on these devices is the generation of excitons, and subsequently free electrons and holes in the polymer. Photons with lower energy can still be absorbed in the polymer (albeit at a much lower rate than the high energy photons), thereby creating excitons, and causing the effects we have described above, but to a much smaller degree as compared to the effects caused by the strongly absorbed photons.

A useful figure merit of a photodetector is the responsivity (R in A/W) of the device, which is a measure of the photo-induced signal of the device compared to the input power from the source being detected and is defined as [35]

$$R = \frac{I_{\text{ph}}}{P_{\text{inc}}} = \frac{I_{\text{Dillum}} - I_{\text{Ddark}}}{E \times A} \quad (5)$$

where I_{ph} is the drain photocurrent, P_{inc} is the optical power incident on the channel of the device, I_{Dillum} is the drain current under illumination, I_{Ddark} is the drain current in the dark, E is the irradiance of the incident light, and A is the effective device area [25]. A plot of R versus gate bias for different wavelengths of incident illumination and a plot of R versus photon energy for different gate biases are shown in Figs. 3 and 4, respectively. From these figures, we see that the responsivity increases as the device is biased into the strong accumulation regime and illuminated by strongly absorbed illumination. In fact, we observe a responsivity greater than 1 A/W for devices used under these conditions, which is comparable to the responsivities of other reported organic photodetectors [9]–[11], [21]. For the case of the dependence on the photon energy, shown in Fig. 4, the higher energy photons, which are strongly absorbed in the polymer, increase the carrier densities in the polymer, as described earlier. In the strong accumulation regime, the photogenerated holes are accumulated into the channel by the applied gate bias and cause an increase in the drain photocurrent, which, in turn, causes an increase in the responsivity. In the OFF-state, fewer holes are accumulated into the channel, therefore, the drain photocurrent and responsivity are observed to be lower in this operating regime.

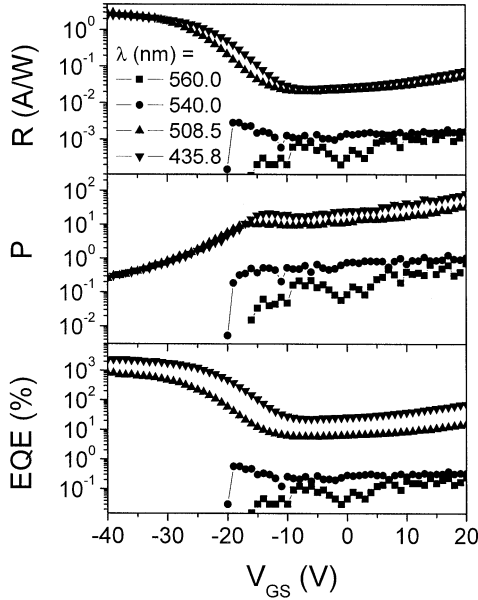


Fig. 3. Responsivity (R), photosensitivity (P) and external quantum efficiency (EQE) versus V_{GS} of the OP-TFT for illumination at different wavelengths/photon energies with $W = 56 \mu\text{m}$, $L = 6 \mu\text{m}$, and $V_{DS} = -10 \text{ V}$.

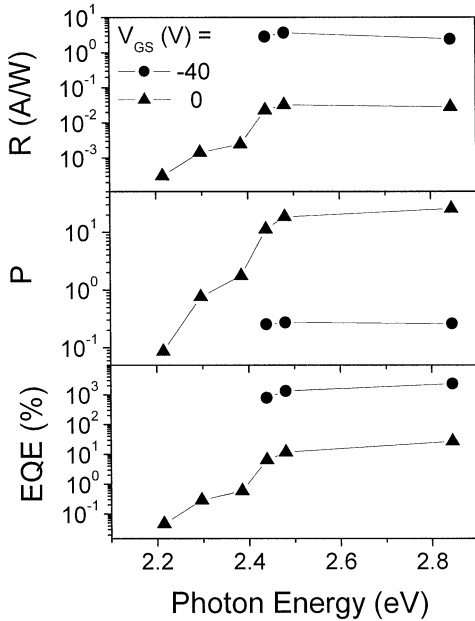


Fig. 4. Responsivity (R), photosensitivity (P) and external quantum efficiency (EQE) versus the energy of incident photons (constant optical flux of 5×10^{13} photons/cm²s) for different biasing regimes of an OP-TFT with $W = 56 \mu\text{m}$, $L = 6 \mu\text{m}$, and $V_{DS} = -10 \text{ V}$.

A second useful figure of merit is the photosensitivity (P), or signal (photo-current) to noise (dark-current) ratio, of the device, which can be approximated as [35]

$$P = \frac{\text{signal}}{\text{noise}} \approx \frac{I_{\text{ph}}}{I_{\text{Ddark}}} \quad (6)$$

For the calculation of P of our devices, we approximate the signal as the drain photocurrent of the illuminated device and the noise as the drain current of the device in the dark. The dependence of the photosensitivity on the applied gate voltage for

different incident wavelengths of illumination and on the energy of the incident photons for different gate biases are shown in Figs. 3 and 4, respectively. We observe that the photosensitivity increases as the device is biased from the strong accumulation regime into the OFF-state and illuminated by strongly absorbed illumination. This is the expected result, and can be explained by examining (6). Since the noise of this detector is related to the dark current, we expect the photosensitivity to be lower in the operating regimes where the dark current is the largest, i.e., in the strong accumulation regime, which is the observed result shown in Fig. 4. The photosensitivity is relatively independent of the applied gate bias when the device is biased in the OFF-state. For the irradiance values used in this experiment, we find a photosensitivity near 100 for a device biased in the OFF-state.

In order to evaluate the overall efficiency of the photodetector in converting an incident optical signal (photons) into an electrical signal (electrons and holes) and allow the comparison of the performance to other photodetectors, we can determine the external quantum efficiency (EQE) of the photodetector, which is defined as [35]

$$EQE = \frac{\frac{I_{\text{ph}}}{q}}{\frac{P_{\text{inc}}}{h\nu}} \quad (7)$$

and corresponds to the number of collected charge carriers compared to the number of incident photons. The dependence of EQE on photon energy for different gate biases and on gate bias for different incident wavelengths is shown in Figs. 3 and 4, respectively. We see from these figures that the EQE increases as the device is biased from the OFF-state into the strong accumulation regime and is larger for strongly absorbed illumination. In fact, an EQE greater than 100% is found for a device biased in the strong accumulation regime and subjected to strongly absorbed illumination. For the case of strongly absorbed photons, the same flux of photons is converted to a higher density of charge carriers inside the polymer, and the EQE of the device is higher, as we expect. As with the responsivity, the device is expected to accumulate and collect the excess, photogenerated holes more efficiently in the strong accumulation regime.

Several comments should be made with regards to the measurements and calculations performed to find the EQE (as well as the other figures of merit) of these devices. As noted previously, under illumination, OP-TFTs exhibit shifts in their electrical characteristics that are believed to be due to the increased carrier concentration and subsequent trapping of charge carriers. These effects, which are similar to the memory effect or persistent photoconductivity which has been observed in organic materials [36]–[39], are not instant compared to the timescale of the measurement and accumulate as the measurement proceeds. These effects are characterized by an accumulating change in the conductivity of the polymer film as it is exposed to illumination, which persists after the illumination has been removed. The polymer can be annealed, as described earlier, to facilitate relaxation to the original state, and allow better comparison of subsequent measurements. In order to overcome the cumulative effects described here, which build up as the measurement progresses, pulsed-gate and pulsed-illumination experiments need to be performed.

Another useful figure of merit, the noise-equivalent power (NEP in $WHz^{-0.5}$), is a measure of the minimum detectable optical power or the optical power required to produce a signal-to-noise ratio of unity. The NEP can be defined as [40]

$$NEP = \frac{I_N}{R} = \frac{I_N \times P_{inc}}{I_{ph}} \quad (8)$$

where I_N is the noise current. For the determination of NEP , we used a calculated value for the noise current of the device that took into consideration the shot (or generation-recombination) noise and Johnson noise, referenced to a bandwidth of 1 Hz. We determined the dependence of NEP on applied gate bias for different illumination wavelengths and incident photon energy for different gate biases. The NEP remains flat, with a value of approximately $10^{-14} WHz^{-0.5}$, as the device is biased from the strong accumulation regime into the OFF-state and when illuminated by light which is strongly absorbed. Since the noise current is related to the drain current of the device, it is expected to be larger in the strong accumulation regime than in the OFF-state. From Fig. 3, we see that the responsivity of the devices shows a similar variation. The result is an NEP that has little variation on the applied gate bias. The NEP is reduced for higher energy photons, since the noise current remains the same but the responsivity is increased for the higher energy photons, as described previously.

We can also define the specific detectivity (D^*) for these devices as [40]

$$D^* = \frac{\sqrt{A}\sqrt{\Delta f}}{NEP} \quad (9)$$

where A is the effective area of the device and Δf is the referenced bandwidth ($= 1$ Hz). For an incident wavelength of 500 nm, we find the specific detectivity of a device (in both the OFF-state and ON-state) to be approximately $2 \times 10^{11} cm Hz^{0.5} W^{-1}$.

B. Dependence on Irradiance

To investigate the effects of monochromatic illumination further, we again measured the transfer characteristics of an OP-TFT under illumination at a wavelength of 460 nm, at different levels of irradiance. This type of experiment allowed us to explore the dependence on the number of absorbed photons, since at larger irradiance levels, it is expected that more photons are absorbed in the polymer film. These results are shown in Fig. 5, where we plot the threshold-voltage normalized, linear regime transfer characteristics. We chose to use 460 nm because it lies in the absorption peak of F8T2, and allowed a larger range of incident, and therefore absorbed, optical flux. We can see, from Fig. 5, that the effects of the illumination increase (i.e., the OFF-state drain current increases and the threshold voltage is reduced) as the irradiance is increased, similar to the effects of broadband illumination [25]. This is the expected effect, since as the irradiance is increased, the polymer film is exposed to a higher flux of photons, thereby generating more charge carriers. The increased number of electrons causes a greater reduction of the threshold voltage, by the neutralization of the positively charged traps, while the increased number of holes causes the channel to have a higher conductivity. And, again,

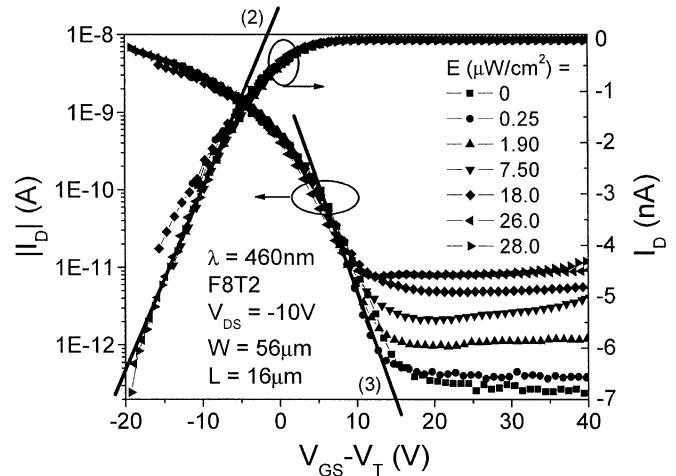


Fig. 5. Threshold voltage-normalized transfer characteristics of OP-TFT illuminated at a wavelength of 460 nm (corresponding to maximum absorption of the F8T2 polymer film) for different irradiance levels. The straight lines are fits using (2) and (3).

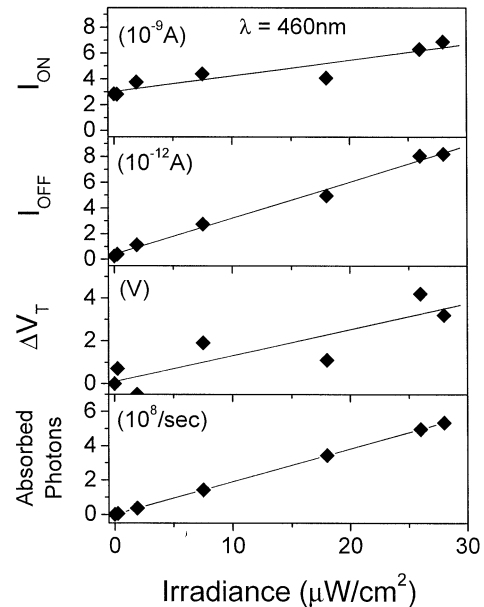


Fig. 6. Dependence of ON-state drain current, OFF-state drain current and the change in threshold voltage on irradiance at a wavelength of 460 nm. Also shown is the number of photons absorbed in the channel region of the device as a function of incident irradiance.

we see that the field-effect mobility and subthreshold swing are not affected by the illumination and have no dependence on the incident irradiance as can be deduced from Fig. 5 [note the slopes of the lines labeled (2) and (3)]. The dependence of the change in threshold voltage, ON-state and OFF-state drain currents, and number of absorbed photons on the incident irradiance are shown in Fig. 6. Note that each parameter plotted in Fig. 6 has a linear relationship with the number of incident photons and, assuming that the absorption coefficient is not strongly dependent on the incident photon flux in the range we use here, this is evidence that the observed effects described above are related to the number of absorbed photons.

In Fig. 7, we plot the responsivity [found using (5)] and photosensitivity [found using (6)] of the device as a function of

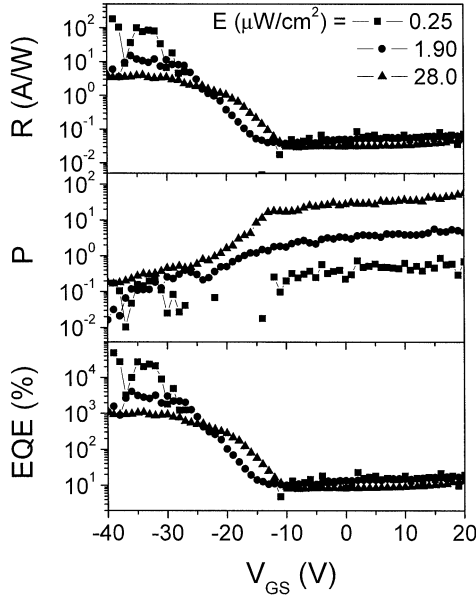


Fig. 7. Responsivity (R), photosensitivity (P) and external quantum efficiency (EQE) of an OP-TFT versus V_{GS} for various irradiance levels at a wavelength of 460 nm with $W = 56 \mu\text{m}$, $L = 6 \mu\text{m}$, and $V_{DS} = -10 \text{ V}$.

applied gate bias for various irradiance levels. With the caveats stated earlier, regarding the memory effect of illuminated organic materials, we see that the responsivity reaches values greater than 1 A/W in the strong accumulation regime and is reduced as the device is biased into the OFF-state. We can also see that the responsivity is highest for the lower irradiance levels. It is possible that this effect is due to the saturation of the drain photocurrent in the strong accumulation regime, even at low incident irradiance levels. Therefore, in the strong accumulation regime, the drain current is expected to be similar for each irradiance level, and the calculated responsivity is expected to be governed by the value of the irradiance. The photosensitivity increases as the device is biased from the strong accumulation regime into the OFF-state, is largest for the highest irradiance level, and is relatively independent of the applied gate bias in the OFF-state, corresponding to the explanation we have presented previously.

In Fig. 7, we also plot the EQE [found using (7)] of the device as a function of applied gate bias for various irradiance levels. From this figure, we see that the EQE decreases as the device is biased from the strong accumulation regime to the OFF-state. At larger gate biases, more of the photogenerated holes are accumulated and contribute to the drain photocurrent, therefore, the efficiency of the device is higher in the strong accumulation regime as compared to the OFF-state. We see from Fig. 7 that as the irradiance is increased, the EQE decreases. For the case of these measurements, we are using a constant illumination wavelength, and, therefore, a constant photon energy. With the assumption that the absorption coefficient is not dependent on the incident irradiance, we see from Fig. 6 that the number of absorbed photons retains a linear relationship with the incident irradiance. Therefore, we speculate that at the higher irradiance values, phenomena such as exciton-exciton annihilation and electron-hole recombination occur, reducing the number of photogenerated carriers that can contribute

to the drain photocurrent. This, in turn, reduces the external quantum efficiency. We observed a nearly linear increase of NEP with irradiance from approximately 3×10^{-15} to $1 \times 10^{-14} \text{ WHz}^{-0.5}$ over the range of irradiance used here, at a wavelength of 460 nm. Processes such as exciton annihilation or carrier recombination effectively reduce the signal that is detected by the device (i.e., the drain photocurrent is smaller than if no recombination occurs). Since the NEP is a measure of the smallest detectable optical power, if the signal is reduced in the device due to these nonidealities, the NEP is expected to increase.

Another measure, which is related to the photosensitivity, is the ratio of total drain current under illumination to drain current in the dark, which is referred to as the photoresponse and has been defined as [34]

$$R_{L/D} = \frac{I_{D\text{illum}}}{I_{D\text{dark}}}. \quad (10)$$

$R_{L/D}$ is a useful parameter for extracting more physical parameters from the illuminated versus dark electrical characteristics of the OP-TFT. The dependence of $R_{L/D}$ on gate bias and incident photon energy is similar to that of the photosensitivity (i.e., increases from strong accumulation to OFF-state and for strongly absorbed illumination and is independent of the applied gate bias in the OFF-state). $R_{L/D}$ increases from nearly unity in the strong accumulation regime to approximately 75 in the OFF-state (depending on the irradiance level). In the OFF-state, this ratio is relatively independent of the gate bias. In the strong accumulation regime, the density of accumulated carriers is due mainly to the applied gate bias, as opposed to the illumination (for the range of irradiance values use here). In the OFF-state, the photogenerated charge carriers are the major contribution to the free carrier density in the channel, and $R_{L/D}$ is strongly dependent on the incident irradiance. In fact, the ratio exhibits a power law dependence on the irradiance. Therefore, $R_{L/D}$ obeys the following:

$$R_{L/D} \propto E^\gamma. \quad (11)$$

In (11), E is the illumination irradiance and the γ -power exponent is a function of the applied V_{GS} . This follows from a model, which has been developed for the photo-field effect in a-Si:H TFTs [41]–[43]. The major assumptions in this model are that the total density of states around mid-gap are constant, there is a symmetric overlap of donor and acceptor states around mid-gap, and that the field-effect is governed by the bulk states and not by the interface states. It is also assumed that the Fermi level splits into quasi-Fermi levels under illumination, which must be the case for spatially dependent carrier generation, since the carriers need to diffuse and redistribute. These assumptions do not seem unreasonable for organic materials, therefore, we assume this model to be valid for OP-TFTs, and the results are shown in Fig. 8. The dependence of γ on V_{GS} can be described using the following:

$$\gamma(V_{GS}) = \begin{cases} \gamma_0 \left(\frac{V_{GS} - V_{GS}}{V_{GS} - V_{FB}} \right), & \text{for } V_{GS} < V_{FB} \\ \gamma_0, & \text{for } V_{GS} > V_{FB}. \end{cases} \quad (12a) \quad (12b)$$

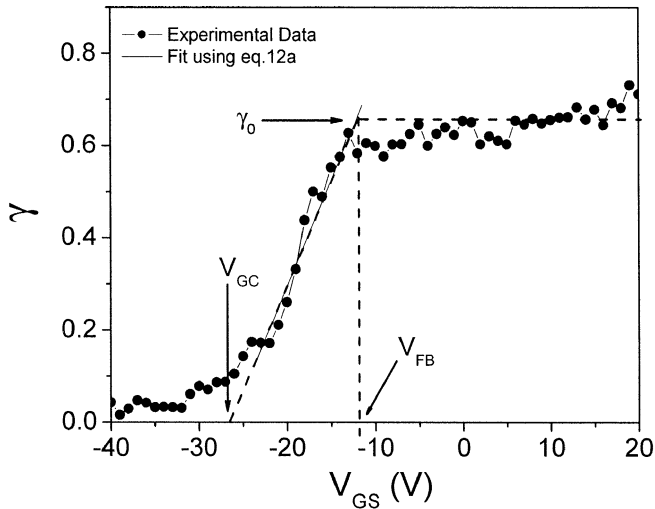


Fig. 8. Gamma factor of the OP-TFT versus V_{GS} for various irradiance levels at a wavelength of 460 nm.

In (12a) and (12b), γ_0 is a material dependent constant, V_{GS} is the applied gate-to-source bias, V_{FB} is the flat-band voltage, and V_{GC} is the critical gate voltage at which the drain current under illumination is ideally equal to the drain current in the dark and is given by

$$V_{GC} = \frac{\sqrt{\epsilon_{\text{semi}} d_{\text{ins}} \beta}}{\sqrt{\epsilon_{\text{ins}}}}. \quad (13)$$

In (13), ϵ_{semi} is the dielectric constant of the semiconductor ($= 2.6$), ϵ_{ins} is the effective dielectric constant of the insulator ($= 2.3$), d_{ins} is the effective thickness of the insulator ($= 2700 \text{ \AA}$) and β is defined as

$$\beta = \frac{(2N_f)^{3/2}}{L} \quad (14)$$

where L is the linear slope of the localized state distribution near the middle of the supposed bandgap and $2N_f$ is the total density of states at midgap. In Fig. 8, we see that we can fit our data in the region $V_{FB} < |V_{GS}| < V_{GC}$ using (12a) with V_{GC} equal to approximately -27 V . This gives a β value of approximately 9.4×10^5 . If we assume a value of $10^{18} \text{ cm}^{-3} \text{ eV}^{-1}$ for $2N_f$ (estimated from (4) with $N_{SS} = 0$), we find that L is equal to $1.1 \times 10^{21} \text{ cm}^{-3} \text{ eV}^{-2}$ from (14). Note that this simple calculation assumes that $N_{SS} = 0$. If $N_{SS} > 0$, then both N_f and L will be reduced to maintain the constant value of β . In the case of our devices, γ_0 from experimental data is approximately 0.6, while the fit using (12b) gives a γ_0 value of approximately 0.7.

It is possible to determine the flat-band voltage (V_{FB}) of the OP-TFT from Fig. 8 using a method similar to that of Schropp *et al.* [42], [43]. The density of accumulated holes in the channel does not increase for applied gate biases from the flat-band voltage to more positive voltages and the source and drain electrodes block electrons coming from the conduction band (LUMO). Therefore, the ratio of drain current under illumination over drain current in the dark is constant for positive applied gate biases. As the gate is biased from the flat-band

voltage to more negative biases, the logarithm of the current ratio is approximately proportional to $V_{GS} - V_{FB}$. As did Schropp *et al.*, we assume that there is no shift in the flat-band voltage under illumination. We extract the flat-band voltage from the crossing point of (12a) and (12b), and we find the V_{FB} of this device to be equal to -12 V .

VI. CONCLUSION

We have studied the electrical performance of F8T2-based OP-TFTs under monochromatic illumination, and have examined their performance as photodetectors. For these devices, the major effect of the absorbed light is a significant increase in the OFF-state drain current and a reduction of the threshold voltage by several volts, depending on the illumination conditions. The field-effect mobility and subthreshold swing are not affected by the illumination. These effects are explained by the photo-generation of excitons in the polymer, which diffuse and dissociate into free charge carriers. The effects on the OFF-state drain current and threshold voltage are dependent on the wavelength and irradiance of the incident illumination. Photons with energy below the optical-gap of the polymer are weakly absorbed, generating few excitons, and therefore have little effect on the electrical characteristics of the OP-TFT. Whereas, higher energy photons are more strongly absorbed in the polymer, generating a higher density of excitons, and causing larger changes in the electrical characteristics. This explanation is confirmed by examining the effects of the level of irradiance at a single photon energy on the electrical characteristics of the OP-TFTs.

We have also presented the relevant photodetector figures of merit, such as the responsivity (R), photosensitivity (P), external quantum efficiency (EQE), and noise-equivalent power (NEP) of these devices, with typical values greater than 1 A/W, 100, 100%, and less than $10 \text{ fWHz}^{-0.5}$, respectively, depending on the illumination and bias conditions. The dependence of these parameters on photon energy, irradiance, and applied gate bias have also been presented and explained.

We propose the use of a model developed for a-Si:H TFTs under illumination to aid in the description of the effects of illumination on the OP-TFTs. Our results agree well with this proposed model. Using this method, we find a flat-band voltage (V_{FB}) of approximately -12 V for these F8T2-based OP-TFTs.

ACKNOWLEDGMENT

The authors would like to thank The Dow Chemical Company for the organic polymer (F8T2) used in this research, Prof. J. Phillips for useful suggestions, S. Kennerly for useful discussions, and the reviewers for constructive comments on the drafts of this paper.

REFERENCES

- [1] C. D. Dimitrakopoulos and D. J. Mascaro, "Organic thin-film transistors: A review of recent advances," *IBM J. Res. Dev.*, vol. 45, pp. 11–27, 2001.
- [2] G. Horowitz, "Organic field-effect transistors," *Adv. Mater.*, vol. 10, pp. 365–377, 1998.
- [3] T. N. Jackson, Y. Lin, D. J. Gundlach, and H. Klauk, "Organic thin-film transistors for organic light-emitting flat-panel display backplanes," *IEEE J. Select. Topics Quantum Electron.*, vol. 4, pp. 100–104, Jan./Feb. 1998.

- [4] H. Sirringhaus, N. Tessler, and R. H. Friend, "Integrated optoelectronic devices based on conjugated polymers," *Science*, vol. 280, pp. 1741–1743, 1998.
- [5] S. R. Forrest, "Active optoelectronics using thin-film organic semiconductors," *IEEE J. Select. Topics Quantum Electron.*, vol. 6, pp. 1072–1083, Nov./Dec. 2000.
- [6] P. Peumans, A. Yakimov, and S. R. Forrest, "Small molecular weight organic thin-film photodetectors and solar cells," *J. Appl. Phys.*, vol. 93, pp. 3693–3723, 2003.
- [7] D. Natali and M. Sampietro, "Detectors based on organic materials: Status and perspectives," *Nucl. Instrum. Meth. A*, vol. 512, pp. 419–426, 2003.
- [8] J. Y. Park, H. M. Le, G. T. Kim, H. Park, Y. W. Park, I. N. Kang, D. H. Hwang, and H. K. Shim, "The electroluminescent and photodiode device made of a polymer blend," *Synth. Met.*, vol. 79, pp. 177–181, 1996.
- [9] J. Gao, F. Hide, and H. Wang, "Efficient photodetectors and photovoltaic cells from composites of fullerenes and conjugated polymers: Photoinduced electron transfer," *Synth. Met.*, vol. 84, pp. 979–980, 1997.
- [10] K. S. Narayan and T. B. Singh, "Nanocrystalline titanium dioxide-dispersed semiconducting polymer photodetectors," *Appl. Phys. Lett.*, vol. 74, pp. 3456–3458, 1999.
- [11] G. Yu, Y. Cao, J. Wang, J. McElvain, and A. J. Heeger, "High sensitivity polymer photosensors for image sensing applications," *Synth. Met.*, vol. 102, pp. 904–907, 1999.
- [12] G. Yu, G. Srdanov, J. Wang, H. Wang, Y. Cao, and A. J. Heeger, "Large area, full-color, digital image sensors made with semiconducting polymers," *Synth. Met.*, vol. 111–112, pp. 133–137, 2000.
- [13] P. Peumans, V. Bulović, and S. R. Forrest, "Efficient, high-bandwidth organic multilayer photodetectors," *Appl. Phys. Lett.*, vol. 76, pp. 3855–3857, 2000.
- [14] J. M. Lupton, R. Koeppel, J. G. Müller, J. Feldmann, U. Scherf, and U. Lemmer, "Organic microcavity photodiodes," *Adv. Mater.*, vol. 15, pp. 1471–1474, 2003.
- [15] R. A. Street, J. Graham, Z. D. Popovic, A. Hor, S. Ready, and J. Ho, "Image sensors combining an organic photoconductor with a-Si:H matrix addressing," *J. Non-Cryst. Sol.*, pp. 1240–1244, 2002.
- [16] R. Rinaldi, E. Branca, R. Cingolani, S. Masiero, G. P. Spada, and G. Gottarelli, "Photodetectors fabricated from a self-assembly of a deoxyguanosine derivative," *Appl. Phys. Lett.*, vol. 78, pp. 3541–3543, 2001.
- [17] D. Natali, M. Sampietro, M. Arca, C. Denotti, and F. A. Devillanova, "Wavelength-selective organic photodetectors for near-infrared applications based on novel neutral dithiolenes," *Synth. Met.*, vol. 137, pp. 1489–1490, 2003.
- [18] T. Zukawa, S. Naka, H. Okada, and H. Onnagawa, "Organic heterojunction phototransistor," *J. Appl. Phys.*, vol. 91, pp. 1171–1174, 2002.
- [19] J. H. Schön and C. Kloc, "Organic metal-semiconductor field-effect phototransistors," *Appl. Phys. Lett.*, vol. 78, pp. 3538–3540, 2001.
- [20] K. S. Narayan, A. G. Manoj, T. B. Singh, and A. A. Alagiriswamy, "Novel strategies for polymer based light sensors," *Thin Solid Films*, vol. 417, pp. 75–77, 2002.
- [21] K. S. Narayan and N. Kumar, "Light responsive polymer field-effect transistor," *Appl. Phys. Lett.*, vol. 79, pp. 1891–1893, 2001.
- [22] S. Martin, J. Y. Nahm, and J. Kanicki, "Gate-planarized organic polymer thin-film transistors," *J. Elect. Mater.*, vol. 31, pp. 512–519, 2002.
- [23] S. Martin and J. Kanicki, "Organic polymer thin-film transistors for active-matrix flat panel displays?," in *Proc. Int. Display Research Conf. (IDRC)*, 2002, pp. 25–28.
- [24] S. Martin, M. C. Hamilton, and J. Kanicki, "Organic polymer thin-film transistors for active-matrix flat panel displays?," *J. SID.*, vol. 11, pp. 543–549, 2003.
- [25] M. C. Hamilton, S. Martin, and J. Kanicki, "Thin-film organic polymer phototransistors," *IEEE Trans. Electron Devices*, vol. 51, pp. 877–885, June 2004.
- [26] A. Salleo and R. A. Street, "Light-induced bias stress reversal in polyfluorene thin-film transistors," *J. Appl. Phys.*, vol. 94, pp. 471–479, 2003.
- [27] R. A. Street, A. Salleo, and M. L. Chabiny, "Bipolaron mechanism for bias-stress effects in polymer transistors," *Phil. Rev. B*, vol. 68, p. 085 316, 2003.
- [28] R. F. Pierret, *Semiconductor Device Physics*. Reading, MA: Addison-Wesley, 1996.
- [29] G. Horowitz and P. Delannoy, "An analytical model for organic-based thin-film transistors," *J. Appl. Phys.*, vol. 70, pp. 469–475, 1991.
- [30] A. Rolland, J. Richard, J.-P. Kleider, and D. Mencaraglia, "Electrical properties of amorphous silicon transistors and MIS devices: Comparative study of top nitride and bottom nitride configurations," *J. Electrochem. Soc.*, vol. 149, pp. 3679–3683, 1993.
- [31] M. C. Hamilton, S. Martin, and J. Kanicki, "Effect of monochromatic illumination on organic polymer thin-film transistors," in *Proc. Int. Display Research Conf. (IDRC)*, 2003, pp. 14–17.
- [32] R. A. Street and A. Salleo, "Contact effects in polymer transistors," *Appl. Phys. Lett.*, vol. 81, pp. 2887–2889, 2002.
- [33] L. Bürgi, T. J. Richards, R. H. Friend, and H. Sirringhaus, "Close look at charge carrier injection in polymer field-effect transistors," *J. Appl. Phys.*, vol. 94, pp. 6129–6137, 2003.
- [34] J. D. Gallezot, S. Martin, and J. Kanicki, "Photosensitivity of a-Si:H TFTs," in *Proc. Int. Display Research Conf. (IDRC)*, 2001, pp. 407–410.
- [35] P. Bhattacharya, *Semiconductor Optoelectronic Devices*, 2nd ed. Englewood Cliffs, NJ: Prentice-Hall, 1997.
- [36] S. Dutta and K. S. Narayan, "Nonexponential relaxation of photoinduced conductance in organic field effect transistors," *Phys. Rev. B*, vol. 68, p. 125 208, 2003.
- [37] A. Fujii, M. Yoneyama, K. Ishihara, S. Maeda, and T. Murayama, "Memory effect of an organic photoconductor and its application to a neuron model," *Appl. Phys. Lett.*, vol. 62, pp. 648–650, 1993.
- [38] M. Hiramoto, T. Imahigashi, and M. Yokoyama, "Photocurrent multiplication in organic pigment films," *Appl. Phys. Lett.*, vol. 64, pp. 187–189, 1994.
- [39] A. Thander and B. Mallik, "Observation of persistent photoconductivity at room temperature in ferrocene-doped poly(methyl methacrylate) thin films containing chloroform molecules," *Solid State Commun.*, vol. 121, pp. 159–164, 2002.
- [40] E. L. Dereniak and D. G. Crowe, *Optical Radiation Detectors*, 1st ed. New York: Wiley, 1984.
- [41] G. Fortunato, L. Mariucci, and C. Reita, "Physics of metal/insulator/amorphous semiconductor structures," in *Amorphous and Microcrystalline Semiconductor Devices—Materials and Device Physics*, J. Kanicki, Ed. Boston, MA: Artech House, 1992.
- [42] R. E. I. Schropp, A. O. Harm, and J. F. Verwey, "A refined theoretical analysis of photofield-effect measurements in a-Si:H thin-film transistors," *Phil. Mag. B*, vol. 53, pp. 431–444, 1986.
- [43] A. O. Harm, R. E. I. Schropp, and F. Verwey, "The photofield effect in a-Si:H thin-film MOS transistors: Theory and measurement," *Phil. Mag. B*, vol. 52, pp. 59–70, 1985.



Michael C. Hamilton (S'97) received the B.S. degree in electrical engineering from Auburn University, Auburn, AL, in 2000, and the M.S. degree in electrical engineering in 2002 from the University of Michigan, Ann Arbor, where he is currently working toward the Ph.D. degree in electrical engineering.

Since 2002, he has been a member of the Organic and Molecular Electronics Research Group, Solid State Electronics Laboratory, Department of Electrical Engineering and Computer Science, University of Michigan. His current research interests include

organic polymer thin-film electronic and optoelectronic devices.



Jerzy Kanicki (M'99–A'99–SM'00) received the Ph.D. degree in sciences from the Free University of Brussels, Brussels, Belgium, in 1982.

He subsequently joined the IBM Thomas J. Watson Research Center, Yorktown Heights, New York, as a Research Staff Member working on hydrogenated amorphous silicon devices for the photovoltaic and flat-panel display applications. In 1994, he joined the University of Michigan as a Professor in the Department of Electrical Engineering and Computer Science. Currently, his research interests

include organic and molecular electronics, thin-film transistors and circuits, and flat-panel displays technology including organic light-emitting devices.